Biomaterials Science

ROYAL SOCIETY OF CHEMISTRY

PAPER

View Article Online
View Journal | View Issue

Open Access Article. Published on 03 March 2026. Downloaded on 6/20/2026 6:10:02 AM.
This article is licensed under a Creative Commons Attribution-NonCommercial 3.0 Unported Licence.

Check for updates

Cite this: *Biomater. Sci.*, 2026, **14**, 2106

Surface modification of intraocular lenses with zwitterionic poly(carboxybetaine) for posterior capsular opacification prevention

Wei Wang,† Jiqiao Qie,† Jiayin Deng,† Yuexin Yang, Haijie Han * and Ke Yao*

Received 9th December 2025,
Accepted 28th February 2026

DOI: 10.1039/d5bm01797a

rsc.li/biomaterials-science

Posterior capsular opacification (PCO) remains the most common long-term complication after cataract surgery, primarily caused by adhesion and proliferation of residual lens epithelial cells (LECs) on the intraocular lens (IOL) surface. Here, we report a zwitterionic carboxybetaine-coating strategy to endow IOLs with anti-adhesive and anti-fibrotic properties without compromising optical clarity. The zwitterionic monomer carboxybetaine methacrylate (CBMA) was grafted onto the IOL surface *via* plasma activation, forming a stable antifouling interface. The CBMA-coated surface exhibited reduced water contact angle and smooth, uniform morphology while preserving optical transparency. Both anti-adhesion assays and IOL implantation studies confirmed that the highly antifouling CBMA coating markedly inhibited LEC adhesion, suppressed PCO formation, and maintained excellent biocompatibility. This work establishes a surface modification approach that integrates zwitterionic chemistry with clinical biomaterials, providing a promising pathway toward next-generation IOLs with intrinsic PCO-preventive functionality.

1. Introduction

Cataract formation is the leading cause of reversible blindness worldwide, characterized by the denaturation and opacification of lens proteins, which obstruct light transmission through the lens and result in visual impairment.[1–3] With the global trend of aging populations, the incidence of cataract continues to rise. At present, the only effective treatment is phacoemulsification to remove the opacified lens, followed by implantation of an intraocular lens (IOL) to restore visual function.[4,5] Despite being well established, this technique still faces major postoperative complications, with posterior capsular opacification (PCO) being the most common and impactful on long-term visual outcomes.[6,7] Clinically, the incidence of PCO within 5 years after surgery ranges from 20% to 40%, while it may be 100% in children, significantly compromising visual quality.[8,9] Although Nd:YAG laser posterior capsulotomy is the standard treatment for PCO, it is an invasive intervention that may cause complications such as retinal detachment, damage to the IOL optic surface, and secondary glaucoma.[10–13] Therefore, preventing the development of PCO has become a major focus in cataract surgery research.

PCO results from the adhesion, migration, proliferation, and epithelial–mesenchymal transition (EMT) of residual lens epithelial cells (LECs) along the interface between the IOL and the capsular bag.[14–16] To reduce the incidence of PCO, extensive efforts have been devoted to improving surgical techniques, optimizing IOL design, and enhancing material properties. To reduce the incidence of PCO, researchers have explored various strategies from multiple perspectives. First, at the surgical level, meticulous removal of cortical remnants and thorough cleaning of the capsular bag can minimize the number of residual LECs, although complete elimination is not feasible.[17] Second, in terms of IOL design, adopting a sharp-edged geometry can create a mechanical barrier that inhibits cellular migration across the IOL edge, but its long-term efficacy remains limited.[18] In addition, the intrinsic material properties of IOLs play a crucial role in PCO development. Although hydrophobic materials are widely used, they often exhibit strong protein adsorption and relatively poor biocompatibility.[19,20] Another key strategy is the drug-eluting functionalization of IOLs, whereby loading agents such as 5-fluorouracil, bromfenac, or cyclosporine A suppress EMT and eradicate residual LECs.[21–25] Although these drug-loading strategies demonstrate promising animal model outcomes, their clinical translation faces significant challenges, including potential biosafety risks of immunosuppressants, complex manufacturing processes, and suboptimal clinical applicability.

In recent years, surface modification of IOLs has emerged as a research focus, as it enables the introduction of specific biological functions while preserving the intrinsic optical and

Eye Center, The Second Affiliated Hospital, School of Medicine, Zhejiang University, Zhejiang Provincial Key Laboratory of Ophthalmology, Zhejiang Provincial Clinical Research Center for Eye Diseases, Zhejiang Provincial Engineering Institute on Eye Diseases, Hangzhou 310009, China. E-mail: hanhj90@zju.edu.cn, xlren@zju.edu.cn
† These authors equally contributed to this work.

This journal is © The Royal Society of Chemistry 2026

Open Access Article. Published on 03 March 2026. Downloaded on 6/20/2026 6:10:02 AM. This article is licensed under a Creative Commons Attribution-NonCommercial 3.0 Unported Licence.

mechanical properties of the material. By altering the chemical composition and interfacial characteristics of the IOL surface, coating modification techniques can effectively modulate surface wettability and cellular behaviors, thereby influencing the adhesion, migration, and proliferation of residual LECs.[26] For instance, hydrophilic molecular coatings such as heparin and polyethylene glycol (PEG) constructed *via* layer-by-layer assembly or surface-initiated reversible addition fragmentation chain transfer polymerization can significantly suppress LEC adhesion through surface energy reduction.[27,28] However, these surface modification technologies still face critical challenges, including complex fabrication processes, stringent preparation conditions, and insufficient long-term stability. Therefore, the development of safe, stable, easy-to-fabricate, and clinically feasible coating systems remains a critical direction in the advancement of IOL surface modification technologies.

Zwitterionic materials have attracted growing interest due to their exceptional resistance to nonspecific biomolecular and cellular adhesion. Zwitterions contain equal numbers of positively and negatively charged moieties while maintaining an overall neutral charge.[29] This unique charge distribution enables strong ion–dipole interactions with surrounding water molecules, leading to the formation of a dense, highly ordered, and energetically stable hydration layer at the material interface.[30] Such a hydration shell imposes a substantial energetic penalty for the approach of proteins or cells, thereby rendering zwitterionic surfaces among the most effective antifouling interfaces currently known.[31,32] Benefiting from this robust hydration mechanism, zwitterionic polymers exhibit outstanding hydrophilicity and ultra-low fouling characteristics, efficiently suppressing the nonspecific adsorption of proteins, bacteria, and mammalian cells.[33,34] This distinct capacity of zwitterionic polymers in minimizing nonspecific interactions is also highly appealing in many *in vivo* applications. For example, zwitterionic hydrogels have been shown to prevent the occurrence of foreign body reactions, including capsule formation for at least 3 months in mice.[35] Compared with conventional heparin and PEG modifications, zwitterionic materials offer several key advantages, including stronger resistance to protein contamination, superior biocompatibility, and markedly improved long-term chemical stability. Their biomimetic charge neutrality, reminiscent of natural cell membranes, further enhances their ability to inhibit cellular adhesion and migration. Consequently, integrating zwitterionic coatings onto the surfaces of IOLs represents a compelling strategy for creating a durable antifouling microenvironment, thereby reducing the attachment and proliferation of LECs and ultimately offering significant potential for the prevention of PCO.

Based on these considerations, the present study employed plasma-induced graft polymerization to covalently anchor the zwitterionic monomer carboxybetaine methacrylate (CBMA) onto the surface of IOL materials, forming a nanoscale, uniformly hydrophilic coating with excellent antifouling and biocompatible properties (Scheme 1A). The CBMA-modified IOLs were systematically evaluated in terms of surface physicochemical characteristics, optical performance, cellular interactions, and *in vivo* anti-PCO efficacy, aiming to explore their potential application in the prevention of secondary cataract (Scheme 1B). This strategy provides a facile and reliable approach for IOL surface functionalization and offers a promising materials-based insight into the prevention of PCO.

2. Materials and methods

2.1. Materials

Carboxybetaine methacrylate (CBMA) was purchased from MedChemExpress (Monmouth Junction, NJ, USA; Cat# HY-W110584). Calcein AM/PI (C2015M) and Cell Counting Kit-8 (CCK-8) assay (C0037) were obtained from Beyotime. DMEM, fetal bovine serum (FBS), trypsin, and penicillin–streptomycin were purchased from Gibco. Ultraviolet quartz slips and polyethylene terephthalate (PET) were used as the experimental substrates in the characterization and *in vitro* cell experiments. Foldable hydrophobic acrylic lenses for animal implantation experiments were supplied by 66 Vision-Tech Co., Ltd (Suzhou, China). MilliQ Water 18.2 (MΩ cm^{-1}) was obtained using a Millipore MilliQ Academic Water Purification System.

2.2. Cell culture

Human lens epithelial cells (HLECs, SRA01-04) were obtained from the RIKEN Cell Bank (RCB1591). The cells were cultured in complete media with 90% DMEM/F12, 9% (v/v) FBS, and 1% penicillin–streptomycin, and passaged with 0.25% trypsin every three days.

2.3. Surface modification of the IOLs

The PET or IOL substrates were rinsed sequentially with absolute ethanol and ultrapure water to remove surface grease and dust. Subsequently, the substrates were placed in a plasma chamber and subjected to surface treatment with air plasma (120 s, 50 W, 0.3 Torr) to generate reactive free radicals on the surface. After plasma activation, the samples were immersed in an aqueous solution containing CBMA at concentrations of

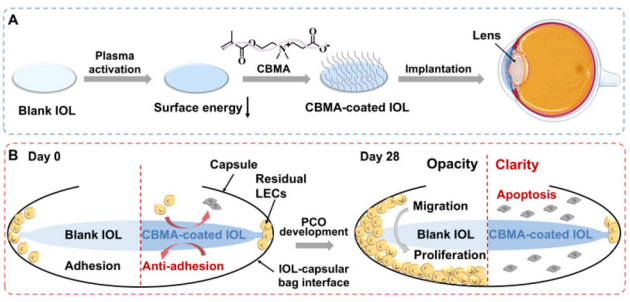

Scheme 1 Schematic of (A) fabrication of antifouling zwitterionic CBMA coating on IOLs and (B) its anti-PCO mechanism *via* reducing residual LEC adhesion.

Open Access Article. Published on 03 March 2026. Downloaded on 6/20/2026 6:10:02 AM. This article is licensed under a Creative Commons Attribution-NonCommercial 3.0 Unported Licence.

2 (CBMA2), 4 (CBMA4), or 8 mg mL^{-1} (CBMA8) to initiate a straightforward one-step free-radical graft polymerization process.

2.4. Characterization of CBMA-modified IOLs

Afterwards, the substrates were dried at room temperature. Water contact angle analysis (WCA, OCA20, Data Physics) was utilized to characterize the surface wettability of the CBMA coating. The optical properties of IOLs, such as light transmittance and imaging quality, were characterized using a microplate reader (M200 PRO NanoQuant, TECAN) and an optical resolution test board, respectively. The appearance of the modified IOLs was examined under a stereomicroscope (SMZ1500, Nikon). The micromorphology of the coatings was observed using a scanning electron microscope (SEM, Phenom Pharos LE, Netherlands) and an atomic force microscope (AFM, Cypher S, Oxford Instruments).

2.5. Evaluation of anti-cell adhesion performances

HLECs were seeded onto the surfaces of unmodified PET (control) and CBMA-modified PET (CBMA2, CBMA4, and CBMA8) to evaluate the cytocompatibility of the materials. After incubation for a predetermined period, cell viability was assessed using a Calcein AM/PI staining kit according to the manufacturer's protocol. Live cells were visualized by green fluorescence, while dead cells were stained red, and representative fluorescence images were captured using a fluorescence microscope (DMI8, Leica) to qualitatively evaluate cell adhesion and viability on each surface.

Quantitative analysis of cell proliferation and metabolic activity was performed using a CCK-8 assay. After incubation with the CCK-8 reagent for the indicated time, the absorbance at 450 nm was measured with a microplate reader. The relative cell viability of each group was normalized to that of the control.

2.6. *In vivo* IOL implantation experiment

New Zealand white rabbits (male, ~2.5 kg) were purchased from the Zhejiang Academy of Medical Sciences (Hangzhou, China).

All animal procedures were performed in accordance with the Guidelines for Care and Use of Laboratory Animals of Zhejiang University and approved by the Animal Ethics Committee of the Second Affiliated Hospital, Zhejiang University School of Medicine (approval number: 2025-322).

Phacoemulsification followed by lens suction was carried out on the right eye of each rabbit under general anesthesia with the help of a phacoemulsification instrument (Fort Worth, TX, Alcon). Polishing of the cortex was shortened for easy establishment of the PCO model. Either untreated or CBMA-modified IOLs were implanted. All surgeries were performed by the same surgeon. After surgery, levofloxacin eye drops, tobramycin–dexamethasone eye drops, compound tropicamide eye drops, and tobramycin–dexamethasone ointment were administered for four weeks with gradually reduced frequency.

2.7. Evaluation of PCO prevention efficacy

Postoperatively, pupil dilation and slit-lamp biomicroscopy were performed on days 3 and 7 to assess acute ocular inflammatory responses. The formation of PCO was further evaluated by slit-lamp examination on day 28 after surgery. Clinical images at each time point were captured using a digital camera mounted on the slit-lamp microscope. After 28 days, the rabbits were anesthetized and euthanized humanely by air embolism. The eyeballs were enucleated and fixed in 10% neutral-buffered formalin for 24 hours. The degree of PCO development within the capsular bag was observed under a stereomicroscope, and the severity of opacification was graded accordingly. The Soemmering's ring and opacity of the posterior capsules were used to assess PCO development. In brief, the lens capsule was divided into 3 portions, including Soemmering's ring, peripheral PCO (PPCO), and central PCO (CPCO). The PCO severity was assessed according to scoring criteria.[36] The intraocular pressure (IOP) was obtained from a portable tonometer. The fixed tissues were embedded in paraffin, sectioned, and subjected to histological analysis. Hematoxylin and eosin (H&E) staining was performed following the manufacturer's instructions.

2.8. *In vivo* biosafety of CBMA-modified IOLs

At postoperative day 28, corneal endothelial morphology and density were assessed using specular microscopy (EM-400, Tomey), and electroretinography (ERG, RETI-Scan21-RETImap, Roland) was performed to evaluate the *in vivo* biocompatibility of the surgery and implanted intraocular lenses. At the end of the observation period, the animals were euthanized, and the eyes were enucleated. The cornea, iris, and retina were carefully dissected, fixed, and processed for histological sectioning to examine tissue morphology.

2.9. Statistical analysis

At least three parallel samples were set up for each group. GraphPad Prism 7 software was used to analyze the experimental results. Data were represented as mean ± standard deviation. Statistical significance was determined using a two-tailed Student's *t*-test for comparisons between two groups, or one-way ANOVA with Tukey's *post-hoc* test for multiple comparisons. $P < 0.05$ (*) was considered statistically significant between the two groups. $P < 0.01$ (**), $P < 0.001$ (***), and $P < 0.0001$ (****) represented significant differences, and $P > 0.05$ (ns) represented non-significance.

3. Results and discussion

3.1. Surface wettability of CBMA-treated substrates

CBMA was grafted onto the substrate after plasma activation, after which surface wettability of the coating was first evaluated. As shown in Fig. 1A, the unmodified substrate exhibited pronounced hydrophobicity, whereas increasing CBMA concentration gradually enhanced surface hydrophilicity. Quantitative WCA measurements (Fig. 1B) showed that the

 This journal is © The Royal Society of Chemistry 2026

Open Access Article. Published on 03 March 2026. Downloaded on 6/20/2026 6:10:02 AM.
This article is licensed under a Creative Commons Attribution-NonCommercial 3.0 Unported Licence.

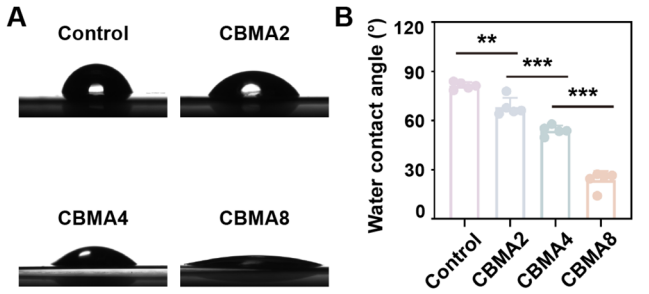

Fig. 1 Surface wettability analysis of CBMA-modified substrates. (A) Representative optical images of water droplets on the PET surfaces for WCA measurements after different treatments. (B) Quantitative analysis of WCA values for the control, CBMA2, CBMA4, and CBMA8 groups (n = 5).

WCA decreased from 81.4 ± 2.2° for the unmodified substrate to 68.3 ± 5.6°, 54 ± 3°, and 23.8 ± 5.5° for the CBMA2, CBMA4, and CBMA8 groups, respectively. These results confirmed that CBMA was successfully grafted onto the substrate surface. Owing to its zwitterionic structure carrying both positive and negative charges, CBMA can form a stable and dense hydration layer in aqueous environments, thereby effectively reducing the surface energy and significantly enhancing the hydrophilicity of the material.

3.2. Morphology of CBMA-modified IOLs

Given that 8 mg mL^{-1} CBMA produced the most significant surface changes, this concentration was selected for morphology and roughness analysis. SEM observations (Fig. 2A) revealed that, in contrast to the smooth surface of the control group, the CBMA-modified surface was uniformly covered by a thin film-like layer. AFM analysis further confirmed these findings (Fig. 2B), showing that the CBMA-modified surface exhibited nanoscale roughness. Collectively, these results demonstrate that CBMA was successfully grafted onto the substrate surface, forming a uniform and stable antifouling coating.

3.3. Optical performance of CBMA coating-modified IOLs

IOLs are critical optical components in cataract surgery, and their optical performance is essential for postoperative visual quality. To evaluate whether CBMA modification affects the optical properties of IOLs, transparency and visible light transmittance tests were performed. As shown in Fig. 3A, both the unmodified and CBMA-modified IOLs exhibited high transparency under a stereomicroscope, with no visible turbidity. Further spectral transmittance analysis (Fig. 3B) revealed that IOLs modified with different concentrations of CBMA showed comparable light transmittance to that of the control group across the visible spectrum (~93%), with no significant differences observed. These findings indicate that although the CBMA coating alters the surface structure at the nanoscale level, it does not adversely affect the optical performance of the IOL, thereby meeting the optical quality requirements for clinical cataract surgery.

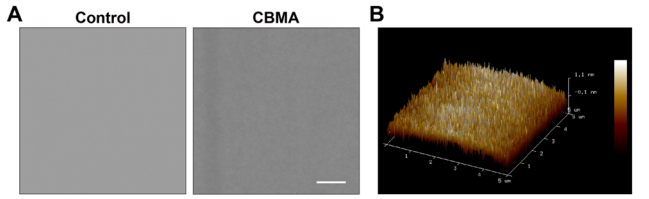

Fig. 2 The surface morphology of IOLs after CBMA modification. (A) The SEM images of the control and CBMA groups (scale bar = 200 nm). (B) The AFM image of the CBMA-modified substrate.

3.4. Anti-adhesion properties of CBMA-modified IOLs

Previous studies have demonstrated that zwitterionic materials can markedly lower interfacial energy and generate highly effective antifouling surfaces, thereby suppressing nonspecific cell adhesion and migration.[37,38] Therefore, this study further evaluated the effects of CBMA modification on the adhesion and proliferation of HLECs. HLECs were seeded onto substrates treated with different concentrations of CBMA, and their morphology and number were observed after 24 hours of culture. As shown in Fig. 4A, the number of adherent cells gradually decreased with increasing CBMA concentration. Consistently, the CCK-8 assay (Fig. 4B) revealed a clear concentration-dependent reduction in cell viability. The control group showed a viability of 99.2 ± 1.3%, which decreased to 95.4 ± 2.4% in the CBMA2 group, 62.5 ± 3.3% in the CBMA4 group, and 19.5 ± 1.3% in the CBMA8 group. These findings indicate

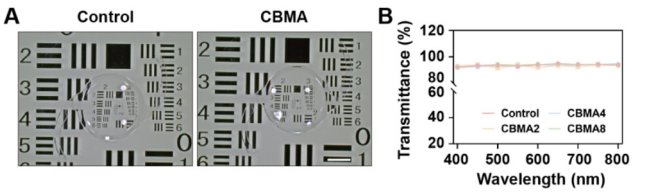

Fig. 3 Optical properties of IOLs after CBMA modification. (A) The macroscopic observation of the IOLs (scale bar = 2 mm). (B) The light transmittance of the control and CBMA-coated materials.

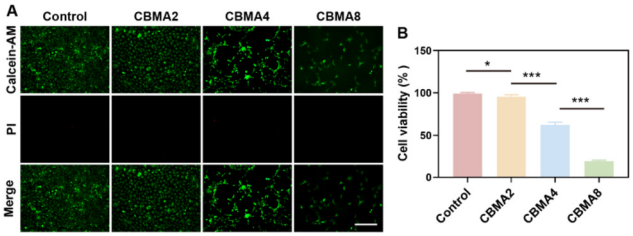

Fig. 4 *In vitro* evaluation of the anti-cell adhesion properties of the CBMA coating. (A) Representative live/dead (Calcein AM/PI) staining images of HLECs exposed to different concentrations of CBMA (0, 2, 4, and 8 mg mL^{-1}). Scale bar = 100 μm. (B) CCK-8 assay results for the various treatment groups (n = 6).

Open Access Article. Published on 03 March 2026. Downloaded on 6/20/2026 6:10:02 AM.
This article is licensed under a Creative Commons Attribution-NonCommercial 3.0 Unported Licence.

that CBMA modification effectively suppresses the adhesion and proliferation of HLECs, suggesting that it may inhibit EMT and fibrosis *in vivo*, thereby mitigating the formation and progression of PCO.

3.5. Evaluation of the anti-PCO efficacy in the animal model

To evaluate the *in vivo* efficacy of CBMA-modified IOLs in preventing PCO, IOLs from different treatment groups were implanted into the eyes of rabbits for postoperative observation. Slit-lamp examinations (Fig. 5A) showed that by postoperative day 7, corneal edema and intraocular inflammation had markedly improved in all groups, reaching comparable baseline conditions. As the observation period progressed, intergroup differences in PCO development became evident. By day 21, the control group exhibited the most rapid and severe PCO progression, while the CBMA4 group showed no significant improvement compared to the control. In contrast, the CBMA8 group demonstrated markedly delayed PCO progression, maintaining a high level of central transparency. As shown in Fig. 5B, the capsule bags in the control and CBMA4 groups displayed marked opacity with prominent Soemmering's ring formation, whereas only peripheral Soemmering's ring formation was observed in the CBMA8 group, and the pupillary center remained clear. These observations were further quantified to evaluate the severity of PCO. As presented in Fig. 5C, the control group showed the highest degree of capsular fibrosis, followed by the CBMA4 group, while the CBMA8 group exhibited the mildest changes. Moreover, the IOP (Fig. 5D) of the experimental animals was monitored during the observation period, and values were maintained within the normal range, indicating that the modeling process was successful and the eye condition of the animals was stable. Histological staining of the capsule bags (Fig. 5E) further confirmed these findings. Extensive fibrotic proliferation (red arrows) was observed in the control and CBMA4 groups, while only mild fibrosis with significantly reduced capsular thickness was seen in the CBMA8 group. Collectively, these results indicate that the CBMA4 group has limited efficacy in preventing PCO, whereas CBMA8 modification markedly inhibits PCO progression. These findings highlight the critical role of surface hydrophilicity enhancement in preventing postoperative PCO formation.

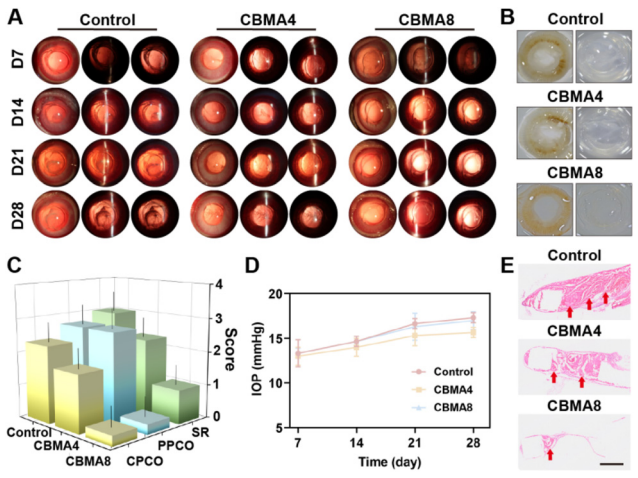

Fig. 5 *In vivo* assessment of PCO suppression in animal models. (A) Representative slit-lamp images at different observation time points (7, 14, 21, and 28 days). (B) Morphological assessment of capsular bags under microscopy. (C) The score of PCO severity for the control, CBMA4, and CBMA8 groups (n = 3). (D) The IOP of all groups during observation (n = 3). (E) H&E-stained images of the posterior capsular bags. Scale bar = 1 mm.

3.6. *In vivo* evaluation of the biocompatibility of CBMA-modified IOLs

Finally, we conducted a comprehensive biosafety evaluation of the CBMA-modified IOLs. First, considering that the ultrasonic energy applied during surgery and the duration of the procedure may affect the corneal endothelium, we examined the morphology and density of corneal endothelial cells.[39] As shown in Fig. 6A and B, endothelial cells in all groups maintained a regular hexagonal arrangement, and the cell density showed no significant difference compared with the normal, non-operated group. These findings indicate that the surgical procedure itself is safe and provide a reliable basis for subsequent assessment of the biocompatibility of CBMA-coated IOLs. Next, we performed ERG examinations on animals implanted with CBMA-modified IOLs. As shown in Fig. 6C, the ERG waveforms were comparable among all groups. Key parameters in ERG include the a-wave, which mainly reflects the activity of cone photoreceptors and Off-bipolar cells, and the b-wave, which originates primarily from the activity of On- and Off-bipolar cells associated with cone photoreceptors. A decrease in the b/a ratio typically suggests impaired cone system function. Therefore, we further quantified the a-wave amplitude, b-wave amplitude, and the b/a ratio. As shown in Fig. 6D–F, the amplitudes of both a- and b-waves were within normal ranges, and no abnormal reduction in the b/a ratio

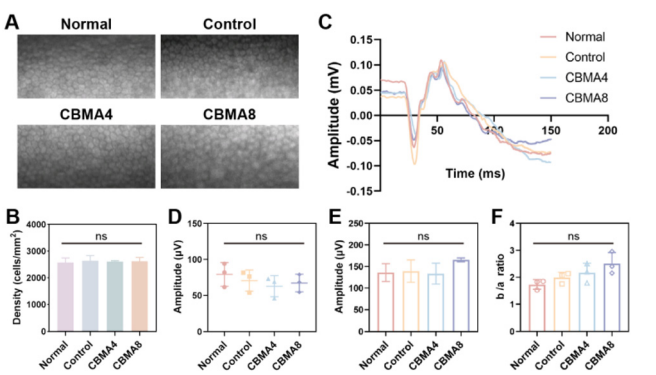

Fig. 6 Assessment of biocompatibility of CBMA-modified IOLs. (A) The morphology of corneal endothelial cells. (B) The density of corneal endothelial cells (n = 3). (C) Retinal electrophysiological assessment. (D) The a-wave of the ERG assessment (n = 3). (E) The b-wave of the ERG assessment (n = 3). (F) The ratio of b-wave/a-wave (n = 3).

This journal is © The Royal Society of Chemistry 2026

Open Access Article. Published on 03 March 2026. Downloaded on 6/20/2026 6:10:02 AM.
This article is licensed under a Creative Commons Attribution-NonCommercial 3.0 Unported Licence.

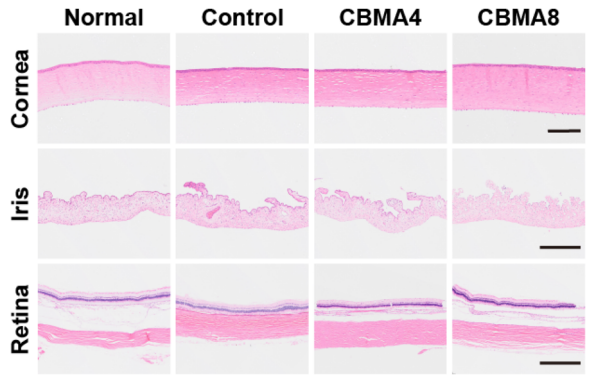

Fig. 7 H&E-stained images of the cornea (scale bar = 200 μm), iris (scale bar = 500 μm), and retina (scale bar = 500 μm).

was observed, indicating that CBMA-modified IOLs did not adversely affect retinal physiological function.

Finally, we conducted histopathological analysis of corneal, iris, and retinal tissues, followed by sectioning and staining. As shown in Fig. 7, the corneal structure remained intact, the iris exhibited normal morphology, and the retinal layers were clearly defined without signs of abnormal tissue or inflammatory reactions. These results further demonstrate that CBMA-modified IOLs exhibit excellent biocompatibility with intraocular tissues.

4. Conclusions

In summary, an antifouling zwitterionic CBMA-based coating was successfully grafted onto IOL surfaces *via* a mild, controllable, and straightforward one-step plasma-initiated grafting process, providing an easy-to-implement method compatible with diverse substrates. The CBMA-modified IOLs maintained excellent optical transparency while exhibiting enhanced surface hydrophilicity. The *in vitro* anti-adhesion tests confirmed that this modification effectively inhibited LEC adhesion and proliferation, thereby preventing and mitigating the development of PCO in the animal model. Owing to the covalent grafting nature of the plasma-induced polymerization, the CBMA coating is expected to exhibit good long-term interfacial stability, which is further supported by its sustained *in vivo* anti-PCO efficacy during the critical postoperative period. These results highlight the potential of CBMA functionalization as a simple and effective surface-engineering strategy to improve the long-term biocompatibility of IOLs. Future work will focus on optimizing the coating stability and investigating its long-term performance and inflammatory responses in larger animal models, paving the way toward clinical translation of inhibiting PCO in hydrophilic IOLs.

Author contributions

Wei Wang and Jiqiao Qie: data curation, formal analysis, investigation, validation, and writing – original draft. Jiayin Deng: data curation, validation, review. Yuexin Yang: methodology, validation. Haijie Han: funding acquisition, methodology, resources, supervision, project administration, validation. Ke Yao: funding acquisition, formal analysis, supervision.

Conflicts of interest

There are no conflicts to declare.

Data availability

All data supporting the findings of this study are available within the article.

Acknowledgements

This work was supported by the Basic Public Welfare Research Plan of Zhejiang Province (LTGY24H120003), the Key Research and Development Project of Zhejiang Province (2024C03073), the National Natural Science Foundation of China (82271063, 82271064), and the Young Elite Scientists Sponsorship Program of the Zhejiang Association for Science and Technology (ZAST). The authors thank Qiong Huang from the Core Facilities, Zhejiang University School of Medicine, for technical support.

References

1 M. V. Cicinelli, J. C. Buchan, M. Nicholson, V. Varadaraj and R. C. Khanna, *Lancet*, 2023, **401**, 377–389.
2 Y.-C. Liu, M. Wilkins, T. Kim, B. Malyugin and J. S. Mehta, *Lancet*, 2017, **390**, 600–612.
3 GBD 2019 Blindness and Vision Impairment Collaborators and Vision Loss Expert Group of the Global Burden of Disease Study, *Lancet Global Health*, 2021, **9**, e144–e160.
4 X. Chen, J. Xu, X. Chen and K. Yao, *Adv. Ophthalmol. Pract. Res.*, 2021, **1**, 100008.
5 D. Allen and A. Vasavada, *Br. Med. J.*, 2006, **333**, 128–132.
6 E. Chan, O. A. R. Mahroo and D. J. Spalton, *Clin. Exp. Optom.*, 2010, **93**, 379–389.
7 I. M. Wormstone, L. Wang and C. S. C. Liu, *Exp. Eye Res.*, 2009, **88**, 257–269.
8 L. M. Nibourg, E. Gelens, R. Kuijer, J. M. M. Hooymans, T. G. van Kooten and S. A. Koopmans, *Exp. Eye Res.*, 2015, **136**, 100–115.
9 A. Medsinge and K. K. Nischal, *Clin. Ophthalmol.*, 2015, **9**, 77.
10 L. Werner, S. K. Pandey, M. Escobar-Gomez, N. Visessook, Q. Peng and D. J. Apple, *Ophthalmology*, 2000, **107**, 463–471.
11 E. Yotsukura, H. Torii, M. Saiki, K. Negishi and K. Tsubota, *J. Cataract Refractive Surg.*, 2016, **42**, 399–404.

Open Access Article. Published on 03 March 2026. Downloaded on 6/20/2026 6:10:02 AM. This article is licensed under a Creative Commons Attribution-NonCommercial 3.0 Unported Licence.

12 J. D. Wesolosky, M. Tennant and C. J. Rudnisky, *J. Cataract Refractive Surg.*, 2017, **43**, 923–928.
13 L. Zhang, R. Shi, X. Chen, X. Gu, J. Shen, A. Wang, S. Ni, L. Cai, H. Guo and J. Yang, *Adv. Ophthalmol. Pract. Res.*, 2025, **5**, 117–123.
14 I. M. Wormstone, Y. M. Wormstone, A. J. O. Smith and J. A. Eldred, *Prog. Retinal Eye Res.*, 2021, **82**, 100905.
15 X. Chen, W. Xiao, W. Chen, X. Liu, M. Wu, Q. Bo, Y. Luo, S. Ye, Y. Cao and Y. Liu, *Cell Death Differ.*, 2017, **24**, 1431–1442.
16 K. K. Youssef and M. A. Nieto, *Nat. Rev. Mol. Cell Biol.*, 2024, **25**, 720–739.
17 J. Qie, S. Wen, Y. Han, S. Liu, L. Shen, H. Chen and Q. Lin, *Biomater. Sci.*, 2022, **10**, 2188–2197.
18 K. Hayashi and H. Hayashi, *Ophthalmology*, 2005, **112**, 1550–1556.
19 D. Liu, J. Tang, L. Shen, S. Liu, S. Zhu, S. Wen and Q. Lin, *Biomacromolecules*, 2022, **23**, 1581–1591.
20 S. Arshinoff, *Can. J. Ophthalmol.*, 2009, **44**, 136–138.
21 J. Xia, Y. Han, L. Shen, R. Wang, S. Wen, S. Zhu and Q. Lin, *Chem. Eng. J.*, 2022, **430**, 132716.
22 X. Zhang, K. Lai, S. Li, J. Wang, J. Li, W. Wang, S. Ni, B. Lu, A. Grzybowski, J. Ji, H. Han and K. Yao, *Bioact. Mater.*, 2022, **9**, 343–357.
23 D. Lu, Y. Han, D. Liu, S. Chen, J. Qie, J. Qu and Q. Lin, *Acta Biomater.*, 2022, **138**, 327–341.
24 X. Zhang, J. Wang, J. Xu, W. Xu, Y. Zhang, C. Luo, S. Ni, H. Han, X. Shentu, J. Ye, J. Ji and K. Yao, *Bioact. Mater.*, 2023, **23**, 539–550.
25 H. Han, S. Li, M. Xu, Y. Zhong, W. Fan, J. Xu, T. Zhou, J. Ji, J. Ye and K. Yao, *Adv. Drug Delivery Rev.*, 2023, **196**, 114770.
26 Y. Zhang, C. Zhang, S. Chen, J. Hu, L. Shen and Y. Yu, *Pharmaceutics*, 2022, **14**, 1343.
27 X. Xu, J.-M. Tang, Y.-M. Han, W. Wang, H. Chen and Q.-K. Lin, *J. Biomater. Appl.*, 2016, **31**, 68–76.
28 Q. Lin, J. Tang, Y. Han, X. Xu, X. Hao and H. Chen, *Colloids Surf., B*, 2017, **151**, 271–279.
29 L. D. Blackman, P. A. Gunatillake, P. Cass and K. E. S. Locock, *Chem. Soc. Rev.*, 2019, **48**, 757–770.
30 B. Li, Z. Yuan, P. Jain, H.-C. Hung, Y. He, X. Lin, P. McMullen and S. Jiang, *Sci. Adv.*, 2020, **6**, eaba0754.
31 S. Jiang and Z. Cao, *Adv. Mater.*, 2010, **22**, 920–932.
32 X. Zhou, W. Cao, Y. Chen, Z. Zhu, Y. Lai, Z. Liu, F. Jia, Z. Lu, H. Han, K. Yao, Y. Wang, J. Ji and P. Zhang, *Acta Biomater.*, 2024, **185**, 226–239.
33 J. B. Schlenoff, *Langmuir*, 2014, **30**, 9625–9636.
34 J. Ladd, Z. Zhang, S. Chen, J. C. Hower and S. Jiang, *Biomacromolecules*, 2008, **9**, 1357–1361.
35 L. Zhang, Z. Cao, T. Bai, L. Carr, J.-R. Ella-Menye, C. Irvin, B. D. Ratner and S. Jiang, *Nat. Biotechnol.*, 2013, **31**, 553–556.
36 Y. Yang, S. Tang, R. Zhang, J. Wang, G. Liu, Y. Han and Q. Lin, *Mater. Des.*, 2025, **260**, 115146.
37 M. He, K. Gao, L. Zhou, Z. Jiao, M. Wu, J. Cao, X. You, Z. Cai, Y. Su and Z. Jiang, *Acta Biomater.*, 2016, **40**, 142–152.
38 Q. Li, C. Wen, J. Yang, X. Zhou, Y. Zhu, J. Zheng, G. Cheng, J. Bai, T. Xu, J. Ji, S. Jiang, L. Zhang and P. Zhang, *Chem. Rev.*, 2022, **122**, 17073–17154.
39 C. Yang, Q. An, H. Zhou and H. Ge, *Adv. Ophthalmol. Pract. Res.*, 2024, **4**, 194–201.

This journal is © The Royal Society of Chemistry 2026